

Quantitative Evaluation of Peptide–Material Interactions by a Force Mapping Method: Guidelines for Surface Modification

Masahito Mochizuki,[†] Masahiro Oguchi,[†] Seong-Oh Kim,^{‡,§} Joshua A. Jackman,^{‡,§} Tetsu Ogawa,[†] Ganchimeg Lkhamsuren,[†] Nam-Joon Cho,^{*,‡,§,||} and Tomohiro Hayashi^{*,†,⊥}

[†]Department of Electronic Chemistry, Interdisciplinary Graduate School of Science and Engineering, Tokyo Institute of Technology, 4259 Nagatsuta-cho, Midori-ku, Yokohama, Kanagawa 226-8502, Japan

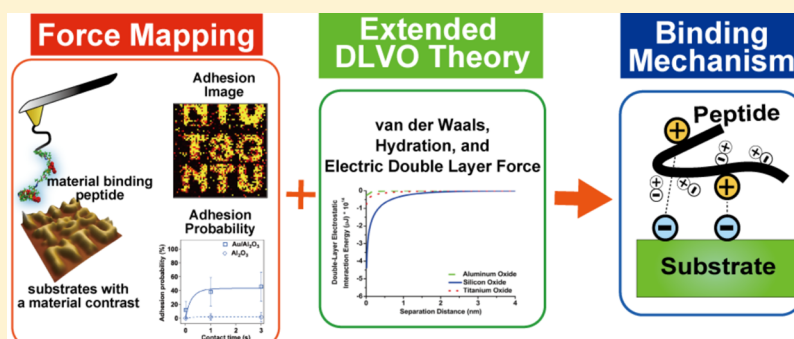
[‡]School of Materials Science and Engineering, Nanyang Technological University, 50 Nanyang Avenue, 639798 Singapore

[§]School of Chemical and Biomedical Engineering, Nanyang Technological University, 62 Nanyang Drive, 637459 Singapore

^{||}Centre for Biomimetic Sensor Science, Nanyang Technological University, 50 Nanyang Drive, 637553 Singapore

[⊥]Surface and Interface Science Laboratory, RIKEN, 2-1 Hirosawa, Wako, Saitama 351-0198, Japan

Supporting Information



ABSTRACT: Peptide coatings on material surfaces have demonstrated wide application across materials science and biotechnology, facilitating the development of nanobio interfaces through surface modification. A guiding motivation in the field is to engineer peptides with a high and selective binding affinity to target materials. Herein, we introduce a quantitative force mapping method in order to evaluate the binding affinity of peptides to various hydrophilic oxide materials by atomic force microscopy (AFM). Statistical analysis of adhesion forces and probabilities obtained on substrates with a materials contrast enabled us to simultaneously compare the peptide binding affinity to different materials. On the basis of the experimental results and corresponding theoretical analysis, we discuss the role of various interfacial forces in modulating the strength of peptide attachment to hydrophilic oxide solid supports as well as to gold. The results emphasize the precision and robustness of our approach to evaluating the adhesion strength of peptides to solid supports, thereby offering guidelines to improve the design and fabrication of peptide-coated materials.

INTRODUCTION

Engineered peptides possessing high and specific affinity to target materials have attracted significant attention in materials science and biotechnology by enabling new functionalities at the nanobio interface, including bioelectronics, biocompatible surface coatings, and anti-infective devices.^{1–4} The target materials include inorganic and organic substrates with diverse properties and surface features.⁵ Although there are a large number of reports on material-binding peptides, the mechanisms underlying the specific interaction between peptide motifs and target materials have been revealed in only a few limited cases.^{6–11} This scarcity reflects the complexity of peptide–material interactions in aqueous solution, which encompass multistep adsorption processes.^{12,13} To elucidate the corresponding mechanisms, precise evaluation of the

interaction can be achieved through various surface-sensitive measurement approaches.

In general, quartz crystal microbalance (QCM) and surface plasmon resonance (SPR) are reliable measurement techniques for determining the attachment of biomacromolecules to a solid support by monitoring the kinetics of adsorption and desorption.^{14,15} However, some material-binding peptide motifs are very small in molecular size and weight (e.g., five to six amino acid residues), resulting in a low signal-to-noise ratio with such methods.¹⁶ Furthermore, these techniques record ensemble-average measurements which can mask critical mechanistic information on the single-molecule level. Taken

Received: May 8, 2015

Revised: June 27, 2015

Published: June 30, 2015

together, these issues may lead to difficulty in systematic quantitative analysis and comparison of experimentally measured binding affinities for different combinations of materials and peptides.

In another promising approach, atomic force microscopy (AFM) enables the highly sensitive measurement of the interaction force between a solid support and peptides tethered to an AFM probe, with pN-level accuracy.¹⁷ Single-molecule force spectroscopy (SMFS) with dynamic force spectroscopy (DFS) has often been employed to analyze specific interactions of ligand–receptor systems.^{18–20} With DFS, the number and positions of the energy potential barriers and the natural lifetime of a bond can be determined. However, the number of binding sites (not the number of energy potential barriers) and association constants cannot be obtained in DFS measurements. Taking into account all of these issues, there is strong motivation to extend the capabilities of AFM force measurements in order to precisely determine the adhesion strength of peptide–material interactions.

Herein, we introduce a quantitative force mapping method to evaluate the binding affinity between peptides and material substrates through statistical analysis of the adhesion force and probability based on AFM measurements conducted at varying probe–surface contact times. In contrast to conventional single-molecule force spectroscopy with DFS as described above, our method does not require optimization of the density of molecules on the apex of the probe in order to detect single-molecule events. In this work, we employ our newly developed method to evaluate the affinity of gold-binding peptide (GBP)²¹ to various oxide materials with several probes each presenting a different number of molecules on the probe apex. The standardization afforded by our approach can lead to a more accurate and robust measurement of the binding affinity of peptides and other biomacromolecules to solid supports.

MATERIALS AND METHODS

AFM Probe Functionalization. For all force measurements, we used Si cantilevers (CSG-01, NT-MDT, Moscow, Russia). The probes were cleaned with a UV–O₃ cleaner (UV-300, SUMCO, Tokyo, Japan). The cleaned probes were first coated with a wetting layer of germanium (thickness 2 nm) by thermal evaporation under vacuum (base pressure 1.0×10^{-4} Pa), followed by the deposition of a gold thin film (thickness 20 nm). After the evaporation process, the probes were immersed in an ethanol solution containing 2-aminoethanethiol (10 mM, Tokyo Chemical Industry, Tokyo, Japan) for 2 h. After immersion, the probes were rinsed with pure ethanol solution and immersed in anhydrous toluene (Wako Chemicals, Tokyo, Japan) solution containing *N*-hydroxysuccinimide-PEG24-maleimide ester (1 mmol/L, Quanta BioDesign, Plain City, OH) for 8 h. After the probes were rinsed with toluene solution, they were immersed for 8 h in PBS buffer solution that contained cysteine-terminated triply repeated in tandem GBP (1 mg/mL, purity >95%, C (MHGKTQATSGTIQS)₃, Scrum, Yokohama, Japan). After immersion, the functionalized probes were rinsed with pure PBS buffer solution. A schematic illustration of the cantilever modified with GBP is shown in Figure 1(a).

AFM Operation. The basic principles of our force measurements are described elsewhere.²² We used a commercial AFM system (MFP-3D, Oxford Instruments, UK). All force measurements were carried out in PBS buffer solution (pH 7.4) which included Tween 20 (0.05 wt %) in order to block hydrophobic interactions between the peptide and probe tip with the substrates that are present due to hydrophobic contaminants on the surfaces. The spring constants of cantilevers were evaluated by measuring the thermal fluctuation of the cantilevers. For acquisition of the force mapping images, force–distance curves were taken at 32×32 or 64×64 points. The scanning area was $90 \times 90 \mu\text{m}^2$. The velocity of the probe approach and the loading rate of the

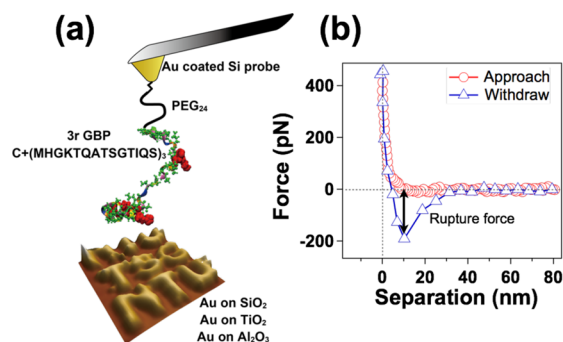


Figure 1. Experimental strategy for quantitative force mapping of peptide–material interactions. (a) Amino acid sequence of gold-binding peptide (GBP) and chemical structure of PEG–GBP moieties immobilized on gold-coated AFM probes. The backbones of the GBP, charged residues, and neutral polar groups are represented by a ribbon, red spheres, and green spheres, respectively. (b) Representative AFM force–distance curves on approach and retraction for a peptide–substrate adhesion event. The definition of adhesion force in this work is indicated by a two-sided arrow.

force on the retraction step were fixed at 2000 nm/s and 400 pN/s, respectively. We controlled the contact time (0.01, 1.01, and 3.01 s) between the probe and substrate with a feedback loop in order to keep the loading force in the range of 400–450 pN (Figure 1(b)).

The letters (N, T, U, T, S, and G) were written with Au over Al₂O₃, TiO₂, and SiO₂ substrates in order to provide distinct areas of surface chemistry for the AFM probe to detect. For the preparation of the substrates, a layer of Al₂O₃ (thickness 100 nm) or TiO₂ (thickness 100 nm) was formed on a clean Si(100) substrate by atomic layer deposition. For the preparation of the SiO₂ substrate, a layer of SiO₂ (thickness 100 nm) was deposited on a cleaned Si wafer with tetraethylorthosilicate using the chemical vapor deposition method.²³ The oxide substrates were masked using photoresist, and then the oxide substrates were coated with chromium (thickness 20 nm) followed by coating with gold (thickness 100 nm) using a thermal evaporation method. After the photoresist mask was removed, the substrates were cleaned by sonication in toluene for 15 min. Note that the different probes were individually prepared for measurements on each substrate; however, an identical procedure was employed in all cases.

Interfacial Force Calculations. To estimate the interaction energy between a single GBP molecule and a solid support, numerical calculations based on the DLVO forces were performed. We assumed that peptide attachment to the solid support can be represented as a sphere in contact with a planar surface. The diameter of the sphere was defined on the basis of the major axis of the peptide. Using this approach, we computed the van der Waals interaction energy and the double-layer electrostatic interaction energy as functions of the separation distance between the sphere and solid support. The material properties of the solid support were varied in order to replicate those of SiO₂, Al₂O₃, or TiO₂. While we do not explicitly calculate the hydration interaction energy due to the lack of reference data for systems of this kind, we may note that this repulsive force is also present and is involved in the stabilization of an attached peptide molecule. Below, we provide more information about the methods of our calculations.

van der Waals Interaction Energy. The van der Waals interaction energy as a function of separation distance between a single GBP molecule and the solid support was calculated by using a classical sphere–plane model. The interaction energy, V_{vdw} , is described by

$$V_{\text{vdw}} = -\frac{AR}{6d} \quad (1)$$

where A is the Hamaker constant of the system, R is the peptide radius, and d is the distance between the surfaces of the sphere and the plane. In the model, the peptide was assumed to be a sphere with $R =$

Table 1. Parameters Used in the van der Waals Interaction Energy Calculations

medium	dielectric constant	oscillator parameter	absorption frequency (UV)	$A_{\nu=0}$ (J)	$A_{\nu>0}$ (J)
anatase TiO ₂ ²⁶	31	4.000	1.27×10^{15}	1.2568×10^{-21}	7.2433×10^{-21}
SiO ₂ ²⁵	3.8	1.098	3.21×10^{15}	2.6724×10^{-21}	1.9800×10^{-21}
Al ₂ O ₃ ²⁷	7	2.096	2.87×10^{15}	2.4443×10^{-21}	6.0380×10^{-21}
peptide ²⁵	3.5	1.041	2.64×10^{15}		
water ²⁵	77.6	0.762	3.17×10^{15}		

3.7 nm. Calculation of the Hamaker constants followed the Prieve and Russell approach,²⁴ as described by eqs 3–6 in ref 25. Table 1 presents a summary of the parameters used in the modeling calculations

The inverse Debye length for our system is calculated by

$$\kappa^{-1} = \sqrt{\frac{\epsilon_r \epsilon_0 k_B T}{2N_A e^2 I}} \quad (2)$$

where I is the ionic strength of the electrolyte in the units of mol/m³, i.e., 150 mol/m³ in the model calculations. T is the temperature of the solution and is 298 K. The calculated inverse Debye length is 1.2805 nm⁻¹.

Double-Layer Electrostatic Interaction Energy. The double-layer electrostatic interaction energy as a function of separation distance between a single GBP molecule and the solid support was calculated by using a classical sphere–plane model, as described by eq 5 in ref 28. The interaction energy, V_{DLE} , is described by

$$V_{DLE} = -\epsilon\pi R[(\psi_1 + \psi_2)^2 \ln(1 - \exp(-\kappa d)) + (\psi_1 - \psi_2)^2 \ln(1 + \exp(-\kappa d))] \quad (3)$$

where ϵ is the dielectric constant of the medium, ψ_1 is the surface potential of the sphere, ψ_2 is the surface potential of the plane, κ is the Boltzmann constant, R is the radius of the sphere, and d is the distance between the surfaces of the sphere and the plane. The surface potential of the GBP molecule was fixed at +10 mV in order to account for its positive net charge. The surface potentials of the solid supports were selected as -26 mV for SiO₂ (ref 29), -5 mV for TiO₂ (ref 30), and 0.4 mV for Al₂O₃ (ref 31) based on values that are reflective of the experimental pH and ionic strength.

RESULTS AND DISCUSSION

Figure 2 presents height (morphology) and adhesion force images of substrates with different combinations of materials measured with GBP-functionalized AFM probes. Convex areas

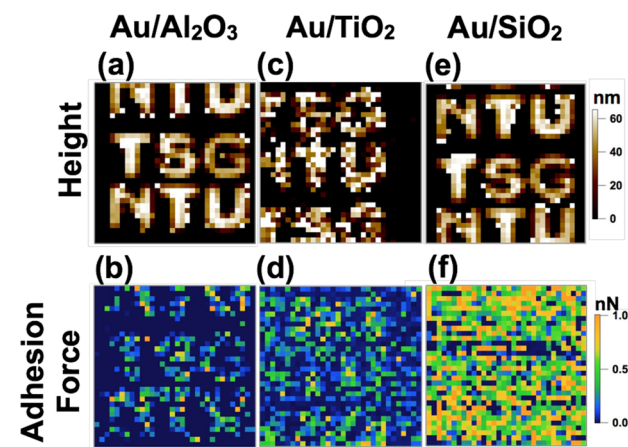


Figure 2. AFM mapping of peptide–material interactions for visualization. Images (32 × 32 pixels) on three substrates with different material combinations, as measured with GBP-functionalized AFM probes in PBS buffer solution: (a, b) Au/Al₂O₃, (c, d) Au/TiO₂, and (e, f) Au/SiO₂. All images are 90 × 90 μm² in size.

on the substrate with a height of about 70 nm consist of Au, and the outer areas are composed of the other materials. As presented in Figure 2, all of the height images exhibit a similar contrast, confirming the uniformity of our fabrication approach. In contrast to the height images, the adhesion force images show clearly different contrasts depending on the combination of materials. That is, the GBP expressed high affinity (high probability and strong adhesion) to Au in all cases, whereas the adhesion observed on other substrate regions depended on the material composition. The highest adhesion contrast was observed for the Au/Al₂O₃ substrate, but the adhesion contrast for the Au/TiO₂ and Au/SiO₂ substrates was smaller.

The contrast in the adhesion images is attributed to the difference in the binding affinity of GBP to the various materials. Qualitatively, of the three hydrophilic oxide materials, GBP demonstrated the strongest affinity for SiO₂ and the weakest affinity for Al₂O₃. Considering the amino acid sequence of the GBP, one GBP molecule on the probe has a net charge of +2 under nearly neutral aqueous buffer conditions. Therefore, GBP is expected to preferentially attach to negatively charged materials by electrostatic attraction. The isoelectric points of SiO₂, TiO₂, and Al₂O₃ are 1.8, 6.7, and 9.1, respectively, and the trend supports the experimental observations.³² Therefore, we conclude that the electrostatic interaction between GBP and the substrate is most attractive for SiO₂, followed by TiO₂ and then Al₂O₃.

To quantitatively compare the results obtained on the three material substrates, we next discuss the kinetics of peptide–substrate attachment. Figure 3 presents the histograms of the adhesion forces observed for GBP and Au (SiO₂/Au substrate) at different contact times. At a contact time of 0.01 s, adhesion events with a rupture force smaller than 50 pN were dominant. With increasing contact time (>1 s), strong adhesion (>100 pN) prevails in the statistical ensembles. The greater adhesion

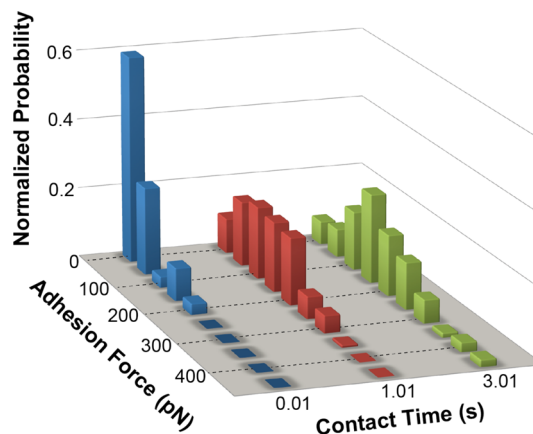


Figure 3. Dependence of peptide–material adhesion force on contact time. Histograms of adhesion forces obtained with three different contact times on the Au/SiO₂ substrate (0.01, 1.01, and 3.01 s).

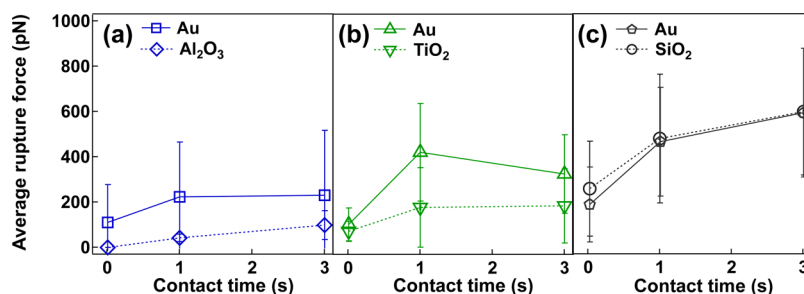


Figure 4. Average adhesion force as a function of contact time. The forces are calculated from the results of the force mapping obtained with the (a) Au/Al₂O₃ substrate, (b) Au/TiO₂ substrate, and (c) Au/SiO₂ substrate in PBS buffer solution. Error bars represent the standard deviations of the measurement results obtained in the three different regions.

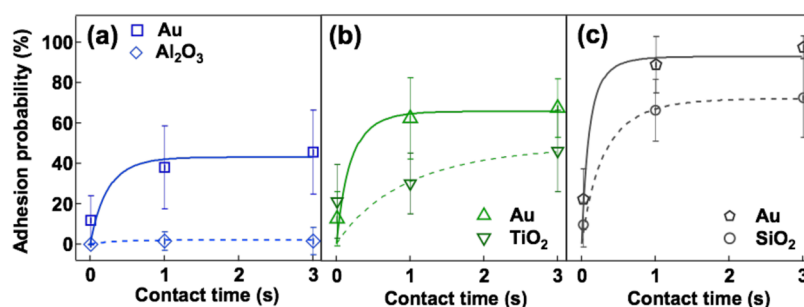


Figure 5. Adhesion probability as a function of contact time. Results are presented for (a) Au and Al₂O₃ on the Au/Al₂O₃ substrate, (b) Au and TiO₂ on the Au/TiO₂ substrate, and (c) Au and SiO₂ on the Au/SiO₂ substrate. Solid and dotted lines are the functions of eq 1 fitted to the experimental results. Error bars represent the standard deviations of the results obtained in the three different regions.

forces measured indicate that the number of attached peptides increases as a function of the contact time on the scale of 1 s.

Figure 4(a–c) presents the average adhesion force as a function of the probe–surface contact time on each material substrate. For all cases, the average adhesion force significantly increased in the first 1 s. We expect that this time progression of the adhesion force was due to conformational changes in attached GBP molecules in order to maximize the attractive interaction energy.²² We also measured the adhesion force with longer contact times of up to 10 s; however, we did not observe a difference in the adhesion forces obtained for contact times of 3 and 10 s. The results demonstrate that the peptide–material attachment is not in equilibrium within 1 s but reaches equilibrium at 3 s. The average adhesion forces for GBP binding to Au at 3 s range between 200 and 600 pN depending on the probe, indicating that the number of molecules involved in the adhesion events varies between the probes. We checked the reproducibility of the density of the peptide moieties on Au surfaces by X-ray photoelectron spectroscopy and determined that there was less than 10% variation in the density of the peptide (N 1s signal). Therefore, we conclude that variations in the average adhesion force are due to the variation in the number of molecules on the probe apex originating not from the density of the molecules but from the shape of the probe apex (Figure S1). As discussed above, a simple comparison of the time progression of the adhesion force does not provide information on the binding affinity of the peptide because the number of peptides involved in the adhesion event is different in each case. To circumvent this issue, we propose to evaluate the binding affinity of GBP to the various material substrates based on the adhesion probability as a function of the contact time.

As presented in Figure 5, the adhesion probabilities, which were evaluated by dividing the number of force curves with

adhesion events by the total number of force curves, monotonically increased as a function of contact time and reached equilibrium at 3 s. The adhesion probability, ρ , is expressed by

$$\rho(t) = 1 - \exp[-m_p m_s A_c^2 K_a^0 \{1 - \exp(-k_d t)\}] \quad (4)$$

where m_p and m_s are densities of binding sites on the probe and substrate, respectively, A_c is the contact area, K_a^0 is the binding affinity, k_d is the dissociation constant, and t is the contact time.^{33,34} First, we fitted the results obtained on the Au surface and assumed the same lumped affinity, $-m_p m_s A_c^2 K_a^0$ and k_d , and different values of A_c for each probe (solid lines in Figure 5(a–c)) and obtained the ratio between A_c among the probes and k_d . Then, we evaluated the $m_p m_s A_c^2 K_a^0$ and k_d values for the Al₂O₃, TiO₂, and SiO₂ substrates (dashed lines in Figure 5). The obtained parameters are summarized in Table 2. We checked the reproducibility of the affinity and dissociation constants calculated from the data sets obtained with different

Table 2. Normalized Lumped Affinity and Dissociation Constants for Peptide–Material Interaction^a

materials	normalized lumped affinity (ratio between $m_p m_s A_c^2 K_a^0$)	dissociation constant (k_d)
Au	1 ± 0.2	3.4 ± 2.0
SiO ₂	0.78 ± 0.16	2.0 ± 1.2
TiO ₂	0.65 ± 0.13	0.79 ± 0.47
Al ₂ O ₃	0.028 ± 0.006	2.73 ± 1.64

^aThe values were obtained from fitting the adhesion probability vs contact time to eq 4. The statistical errors indicate the standard deviation of the fluctuation of the values in the fitting of the adhesion probability to eq 4 within the error bars indicated in Figure 5.

probes, and the deviations are smaller than ± 20 and 65%, respectively.

Finally, we discuss the mechanism underlying the binding interaction between GBP and the materials used in this work. There was no significant difference in k_d among the materials, indicating that the stability of attached peptides is similar.³⁵ This is also rationalized by the results of the experimentally determined adhesion forces. At the contact time of 3 s (equilibrated state), the difference in the adhesion forces is relatively minor compared to large differences in the adhesion probability (Figure 4). Although the large variance in the measured properties renders it difficult to show a difference in the measured k_d values for the limited sample size that was tested in the study, the differences in k_d values alone cannot explain the contrast observed in the adhesion images and the differences in the adhesion probabilities (Figures 2 and 4). Indeed, there exists a correlation between the values of the normalized $m_p m_s K_a^0$ and the adhesion images and probabilities. Therefore, we conclude that $m_p m_s K_a^0$ mainly governs the binding affinity. The positively charged GBP molecules have a greater chance to form ionic bonds with negative deprotonated hydroxyl groups, which are abundant on substrates such as SiO_2 and TiO_2 . Therefore, a high m_s value is expected in PBS buffer solution for such cases. On the other hand, the surface of Al_2O_3 provides less negatively charged binding sites due to hydroxyl group protonation under the solution conditions, which results in a lower lumped affinity.

According to extended-DLVO theory, the peptide–substrate interaction can be described in terms of the balance of three interfacial forces: the van der Waals, double-layer electrostatic, and hydration forces. The attractive van der Waals interaction energy for this system is nearly equivalent for the TiO_2 and Al_2O_3 cases and appreciably smaller for the SiO_2 case (Figure 6(a)). By contrast, the double-layer electrostatic interaction energy is the most attractive in the SiO_2 case and less attractive in the TiO_2 (moderate) and Al_2O_3 (weakest) cases (Figure 6(b)). On the basis of the experimental results which support that peptide attachment is in fact strongest on SiO_2 , the theoretical analysis supports electrostatic interactions playing a key role in mediating peptide attachment. Another important factor is the repulsive hydration force which is appreciably greater on TiO_2 and Al_2O_3 versus SiO_2 , as recently discussed^{36,37} in the context of lipid–substrate interactions on the same set of material substrates. The hydration force arises from the energy required to remove confined interfacial water molecules attached to the oxide film substrates, and the variation in this force among the three substrates is due to the differences in surface polarizability ($\text{TiO}_2 > \text{Al}_2\text{O}_3 > \text{SiO}_2$)³⁸—greater surface polarizability is correlated with the binding strength and thickness of the hydration layer on the substrate.³⁹ When all three interfacial forces are taken into account and viewed collectively, the trends observed in the calculated adhesion forces and probabilities from the AFM measurements are in excellent agreement with theoretical predictions based on extended-DLVO theory. The high affinity of the peptide for SiO_2 over the other two oxide substrates is likely due to the combination of strong electrostatic attraction and a weak repulsive hydration force. Considering that the peptide has the lowest affinity for Al_2O_3 out of the three oxide film substrates, we conclude that the double-layer electrostatic force is the major contributing factor that governs peptide attachment in general. Taken together, these findings provide insight into how the balance of interfacial forces mediates the attachment of

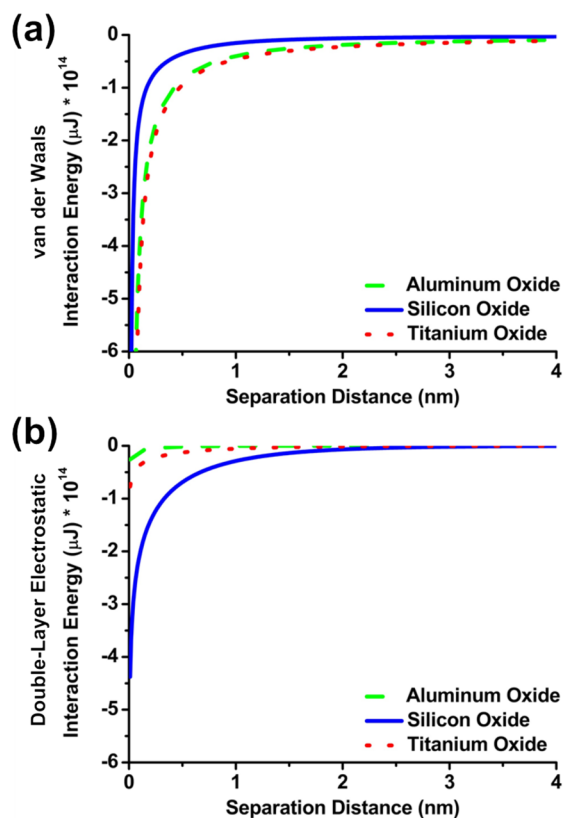


Figure 6. Interaction energies of peptide attachment on material substrates. (a) van der Waals interaction energy as a function of separation distance for a single GBP peptide molecule near a solid support. (b) Double-layer electrostatic interaction energy as a function of separation distance for a single GBP peptide molecule near a solid support.

biomacromolecules to solid supports and validate our AFM-based measurement approach.

From our results (Table 2), the strong affinity between GBP and Au can also be attributed to a large $m_p m_s K_a^0$. In contrast to the oxide substrates, there is no explicit surface charge originating from the ionization of the surface atoms on an Au surface except for accumulated ions from the solution because the gold surface is relatively inert to oxidation under neutral pH conditions. The mechanisms underlying molecular adhesion on gold include charge transfer, van der Waals attraction, and the polarization of gold (image charge effect).^{40–44} In the case of the aforementioned interactions, the gold surface provides binding sites with low positional and orientational dependence, resulting in a larger m_s .⁴⁴ On the basis of the GBP sequence, polar and charged groups are abundant (nine neutral polar, two cationic, and three hydrophobic residues in the repeating unit), which may lead to a larger m_p . In addition, molecular dynamics simulations suggest that the functional groups on peptide chains tend to maximize their interaction with an Au(111) surface by dynamically forming epitaxial configurations.⁴⁵ As a result, the lumped affinity for GBP–Au binding is higher than the affinities of GBP to the oxide film substrates (Table 2). This binding model is also consistent with the model proposed by Sarikaya et al. in which polar groups of peptides were reported to play an anchoring role for highly conductive metals such as Au and Pt.^{45–47}

CONCLUSIONS

In this work, we have developed a quantitative force mapping method to evaluate the binding affinity of material-binding peptides to various materials. We have also demonstrated the application of this approach to evaluating the binding affinity of GBP to Au and hydrophilic oxide film (SiO_2 , TiO_2 , and Al_2O_3) substrates, and we discuss the physical origins underlying the quantitative differences in the adhesion probability and binding affinity of GBP to the different material substrates. One advantage of this approach over a conventional single-molecule force spectroscopic approach is that our approach does not require the optimization of conditions for the preparation of probes to detect single-molecule events. Using several data sets of the probabilities of adhesion to a reference material (Au in this work) and other materials which were measured at different contact times, we can evaluate the binding affinity while taking into account variations in the number of peptides involved in adhesion events. Our experimental findings show excellent agreement with theoretical extended-DLVO calculations and demonstrate that our AFM-based measurement approach can be used to quantitatively measure the adhesion forces associated with the attachment of single biomacromolecules to various materials for various applications such as antifouling coatings and drug delivery.^{48,49}

ASSOCIATED CONTENT

Supporting Information

SEM characterization of the AFM probe functionalization. The Supporting Information is available free of charge on the ACS Publications website at DOI: 10.1021/acs.langmuir.5b01691.

AUTHOR INFORMATION

Corresponding Authors

*E-mail: njcho@ntu.edu.sg.

*E-mail: hayashi@echem.titech.ac.jp.

Notes

The authors declare no competing financial interest.

ACKNOWLEDGMENTS

We acknowledge support from the National Research Foundation (NRF-NRFF2011-01), the National Medical Research Council (NMRC/CBRG/0005/2012), and Nanyang Technological University to N.-J.C. T.H. acknowledges the support of MEXT KAKENHI (grant no. 26282118). The work was also supported by an ASPIRE League Research Grant.

REFERENCES

- (1) Sarikaya, M.; Tamerler, C.; Jen, A. K.-Y.; Schulten, K.; Baneyx, F. Molecular biomimetics: nanotechnology through biology. *Nat. Mater.* **2003**, *2* (9), 577–585.
- (2) Shiba, K. Exploitation of peptide motif sequences and their use in nanobiotechnology. *Curr. Opin. Biotechnol.* **2010**, *21*, 412–425.
- (3) Tamerler, C.; Sarikaya, M. Molecular biomimetics: Genetic synthesis, assembly, and formation of materials using peptides. *MRS Bull.* **2008**, *33* (5), 504–510.
- (4) Tamerler, C.; Sarikaya, M. Molecular biomimetics: Utilizing nature's molecular ways in practical engineering. *Acta Biomater.* **2007**, *3* (3), 289–299.
- (5) Vallee, A.; Humblot, V.; Pradier, C.-M. Peptide interactions with metal and oxide surfaces. *Acc. Chem. Res.* **2010**, *43* (10), 1297–1306.
- (6) Hayashi, T.; Sano, K.; Shiba, K.; Kumashiro, Y.; Iwahori, K.; Yamashita, I.; Hara, M. Mechanism underlying specificity of proteins targeting inorganic materials. *Nano Lett.* **2006**, *6* (3), 515–519.

- (7) Hayashi, T.; Sano, K. I.; Shiba, K.; Iwahori, K.; Yamashita, I.; Hara, M. Critical Amino Acid Residues for the Specific Binding of the Ti-Recognizing Recombinant Ferritin with Oxide Surfaces of Titanium and Silicon. *Langmuir* **2009**, *25* (18), 10901–10906.

- (8) Oren, E. E.; Notman, R.; Kim, I. W.; Evans, J. S.; Walsh, T. R.; Samudrala, R.; Tamerler, C.; Sarikaya, M. Probing the Molecular Mechanisms of Quartz-Binding Peptides. *Langmuir* **2010**, *26* (13), 11003–11009.

- (9) Sultan, A. M.; Hughes, Z. E.; Walsh, T. R. Binding affinities of amino acid analogues at the charged aqueous titania interface: implications for titania-binding peptides. *Langmuir* **2014**, *30* (44), 13321–9.

- (10) Sano, K.-I.; Shiba, K. A Hexapeptide Motif that Electrostatically Binds to the Surface of Titanium. *J. Am. Chem. Soc.* **2003**, *125*, 14234–14235.

- (11) Sano, K.-I.; Sasaki, H.; Shiba, K. Specificity and Biomineralization Activities of Ti-Binding Peptide-1 (TBP-1). *Langmuir* **2005**, *21*, 3090–3095.

- (12) So, C. R.; Tamerler, C.; Sarikaya, M. Adsorption, Diffusion, and Self-Assembly of an Engineered Gold-Binding Peptide on Au (111) Investigated by Atomic Force Microscopy. *Angew. Chem., Int. Ed.* **2009**, *48* (28), 5174–5177.

- (13) So, C. R.; Hayamizu, Y.; Yazici, H.; Gresswell, C.; Khatayevich, D.; Tamerler, C.; Sarikaya, M. Controlling self-assembly of engineered peptides on graphite by rational mutation. *ACS Nano* **2012**, *6* (2), 1648–1656.

- (14) Mermut, O.; Phillips, D. C.; York, R. L.; McCrea, K. R.; Ward, R. S.; Somorjai, G. A. In situ adsorption studies of a 14-amino acid leucine-lysine peptide onto hydrophobic polystyrene and hydrophilic silica surfaces using quartz crystal microbalance, atomic force microscopy, and sum frequency generation vibrational spectroscopy. *J. Am. Chem. Soc.* **2006**, *128* (11), 3598–3607.

- (15) Micksch, T.; Liebelt, N.; Scharnweber, D.; Schwenzer, B. Investigation of the Peptide Adsorption on ZrO_2 , TiZr , and TiO_2 Surfaces as a Method for Surface Modification. *ACS Appl. Mater. Interfaces* **2014**, *6* (10), 7408–7416.

- (16) Chen, H.; Su, X.; Neoh, K. G.; Choe, W. S. QCM-D analysis of binding mechanism of phage particles displaying a constrained heptapeptide with specific affinity to SiO_2 and TiO_2 . *Anal. Chem.* **2006**, *78* (14), 4872–9.

- (17) Samori, P., Ed. *Scanning Probe Microscopies Beyond Imaging*; Wiley-VCH: Weinheim, 2006.

- (18) Evans, E. Introductory Lecture Energy landscapes of biomolecular adhesion and receptor anchoring at interfaces explored with dynamic force spectroscopy. *Faraday Discuss.* **1999**, *111* (0), 1–16.

- (19) Merkel, R.; Nassoy, P.; Leung, A.; Ritchie, K.; Evans, E. Energy landscapes of receptor-ligand bonds explored with dynamic force spectroscopy. *Nature* **1999**, *397* (6714), 50–53.

- (20) Heymann, B.; Grubmüller, H. Dynamic Force Spectroscopy of Molecular Adhesion Bonds. *Phys. Rev. Lett.* **2000**, *84* (26), 6126–6129.

- (21) Tamerler, C.; Duman, M.; Oren, E. E.; Gungormus, M.; Xiong, X. R.; Kacar, T.; Parviz, B. A.; Sarikaya, M. Materials specificity and directed assembly of a gold-binding peptide. *Small* **2006**, *2* (11), 1372–1378.

- (22) Arai, Y.; Okabe, K. I.; Sekiguchi, H.; Hayashi, T.; Hara, M. Nanoscale Chemical Composition Analysis Using Peptides Targeting Inorganic Materials. *Langmuir* **2011**, *27* (6), 2478–2483.

- (23) Becker, F. S.; Pawlik, D.; Anzinger, H.; Spitzer, A. Low-pressure deposition of high-quality SiO_2 films by pyrolysis of tetraethylorthosilicate. *J. Vac. Sci. Technol., B: Microelectron. Process. Phenom.* **1987**, *5* (6), 1555–1563.

- (24) Prieve, D. C.; Russel, W. B. Simplified predictions of Hamaker constants from Lifshitz theory. *J. Colloid Interface Sci.* **1988**, *125* (1), 1–13.

- (25) Tero, R.; Ujihara, T.; Urisu, T. Lipid bilayer membrane with atomic step structure: Supported bilayer on a step-and-terrace TiO_2 (100) surface. *Langmuir* **2008**, *24* (20), 11567–11576.

- (26) Jellison, G.; Boatner, L.; Budai, J.; Jeong, B.-S.; Norton, D. Spectroscopic ellipsometry of thin film and bulk anatase TiO₂. *J. Appl. Phys.* **2003**, *93* (12), 9537–9541.
- (27) Knowles, K. Dispersion forces at planar interfaces in anisotropic ceramics. *J. Ceram. Process. Res.* **2005**, *6*, 10–16.
- (28) Valle-Delgado, J.; Molina-Bolivar, J.; Galisteo-Gonzalez, F.; Galvez-Ruiz, M.; Feiler, A.; Rutland, M. W. Existence of hydration forces in the interaction between apoferritin molecules adsorbed on silica surfaces. *Langmuir* **2005**, *21* (21), 9544–9554.
- (29) Attard, P.; Antelmi, D.; Larson, I. Comparison of the zeta potential with the diffuse layer potential from charge titration. *Langmuir* **2000**, *16* (4), 1542–1552.
- (30) Suttiponparnit, K.; Jiang, J.; Sahu, M.; Suvachittanont, S.; Charinpanitkul, T.; Biswas, P. Role of surface area, primary particle size, and crystal phase on titanium dioxide nanoparticle dispersion properties. *Nanoscale Res. Lett.* **2011**, *6*, 27.
- (31) Bousse, L.; De Rooij, N. F.; Bergveld, P. The influence of counter-ion adsorption on the ψ_0 /pH characteristics of insulator surfaces. *Surf. Sci.* **1983**, *135* (1), 479–496.
- (32) Yoon, R. H.; Salman, T.; Donnay, G. Predicting Points of Zero Charge of Oxides and Hydroxides. *J. Colloid Interface Sci.* **1979**, *70* (3), 483–493.
- (33) Zhu, C.; Williams, T. E. Modeling concurrent binding of multiple molecular species in cell adhesion. *Biophys. J.* **2000**, *79* (4), 1850–1857.
- (34) Lü, S.; Ye, Z.; Zhu, C.; Long, M. Quantifying the effects of contact duration, loading rate, and approach velocity on P-selectin–PSGL-1 interactions using AFM. *Polymer* **2006**, *47* (7), 2539–2547.
- (35) In general, the dissociation constant evaluated by force spectroscopy is 10²–10⁴ times larger than that obtained from the kinetics of adsorption and desorption because of a forced deformation of the potential landscape.
- (36) Jackman, J. A.; Zan, G. H.; Zhao, Z.; Cho, N. J. Contribution of the hydration force to vesicle adhesion on titanium oxide. *Langmuir* **2014**, *30* (19), 5368–5372.
- (37) Jackman, J. A.; Tabaei, S. R.; Zhao, Z.; Yorulmaz, S.; Cho, N. J. Self-Assembly Formation of Lipid Bilayer Coatings on Bare Aluminum Oxide: Overcoming the Force of Interfacial Water. *ACS Appl. Mater. Interfaces* **2015**, *7* (1), 959–968.
- (38) Zhdanov, V.; Kasemo, B. Van der Waals interaction during protein adsorption on a solid covered by a thin film. *Langmuir* **2001**, *17* (18), 5407–5409.
- (39) Reimhult, E.; Höök, F.; Kasemo, B. Intact vesicle adsorption and supported biomembrane formation from vesicles in solution: influence of surface chemistry, vesicle size, temperature, and osmotic pressure. *Langmuir* **2003**, *19* (5), 1681–1691.
- (40) Medeiros, P. V. C.; Gueorguiev, G. K.; Stafström, S. Bonding, charge rearrangement and interface dipoles of benzene, graphene, and PAH molecules on Au(111) and Cu(111). *Carbon* **2015**, *81* (C), 620–628.
- (41) Iori, F.; Corni, S. Including image charge effects in the molecular dynamics simulations of molecules on metal surfaces. *J. Comput. Chem.* **2008**, *29* (10), 1656–1666.
- (42) Iori, F.; Di Felice, R.; Molinari, E.; Corni, S. GoLP: An atomistic force-field to describe the interaction of proteins with Au(111) surfaces in water. *J. Comput. Chem.* **2009**, *30* (9), 1465–1476.
- (43) Hoefling, M.; Iori, F.; Corni, S.; Gottschalk, K.-E. Interaction of Amino Acids with the Au(111) Surface: Adsorption Free Energies from Molecular Dynamics Simulations. *Langmuir* **2010**, *26* (11), 8347–8351.
- (44) Zhong, Z.; Patskovskyy, S.; Bouvrette, P.; Luong, J. H. T.; Gedanken, A. The Surface Chemistry of Au Colloids and Their Interactions with Functional Amino Acids. *J. Phys. Chem. B* **2004**, *108* (13), 4046–4052.
- (45) Heinz, H.; Farmer, B. L.; Pandey, R. B.; Slocik, J. M.; Patnaik, S. S.; Pachter, R.; Naik, R. R. Nature of Molecular Interactions of Peptides with Gold, Palladium, and Pd–Au Bimetal Surfaces in Aqueous Solution. *J. Am. Chem. Soc.* **2009**, *131* (28), 9704–9714.
- (46) Tamerler, C.; Sarikaya, M. Genetically Designed Peptide-Based Molecular Materials. *ACS Nano* **2009**, *3* (7), 1606–1615.
- (47) Seker, U. O. S.; Wilson, B.; Kulp, J. L.; Evans, J. S.; Tamerler, C.; Sarikaya, M. Thermodynamics of Engineered Gold Binding Peptides: Establishing the Structure-Activity Relationships. *Biomacromolecules* **2014**, *15* (7), 2369–2377.
- (48) Hayashi, T.; Hara, M. Nonfouling self-assembled monolayers: mechanisms underlying protein and cell resistance. *Curr. Phys. Chem.* **2011**, *1* (2), 90–98.
- (49) Ding, H.-m.; Ma, Y. Q. Theoretical and computational investigations of nanoparticle-biomembrane interactions in cellular delivery. *Small* **2015**, *11* (9–10), 1055–1071.